Electronic structure of $Ca_3Co_4O_9$ studied by photoemission spectroscopy: Phase separation and charge localization

Y. Wakisaka
Department of Physics, University of Tokyo, Chiba 277-8561, Japan

S. Hirata and T. Mizokawa
Department of Complexity Science and Engineering, University of Tokyo, Chiba 277-8561, Japan

Y. Suzuki, Y. Miyazaki, and T. Kajitani
Department of Applied Physics, Tohoku University, Sendai 980-8579, Japan

(Received 26 September 2008; revised manuscript received 9 November 2008; published 5 December 2008)

We report on an electronic structure study of a quasi-two-dimensional Co oxide $Ca_3Co_4O_9$ with Ca_2CoO_3 rocksalt layers and CoO_2 triangular lattice layers by means of x-ray photoemission spectroscopy (XPS), ultraviolet photoemission spectroscopy (UPS), configuration-interaction calculation on a CoO_6 cluster model, and unrestricted Hartree-Fock calculation on a multiband *d-p* model. The Co 2*p* XPS spectrum shows that the Co valence of the rocksalt layer is similar to that of the triangular lattice layer. The cluster-model analysis of the Co 2*p* XPS spectrum indicates that the Co sites of the rocksalt and triangular lattice layers commonly have charge-transfer energy Δ of $\sim$1.0 eV, *d-d* Coulomb interaction U of $\sim$6.5 eV, and transfer integral $(pd\sigma)$ of ~ -2.3 eV. The Co 3*d* t_{2g} peak in the valence-band XPS spectrum remains sharp even above the spin-state transition temperature at $\sim$380 K, indicating that the spin-state transition is different from the low-spin to intermediate-spin or high-spin transitions in perovskite $LaCoO_3$. The line shape of the UPS spectrum near the Fermi level can be reproduced by the combination of unrestricted Hartree-Fock results for the charge-ordered insulating (COI) and paramagnetic metallic (PM) states. The analysis shows that the phase separation between the COI and PM states plays important roles in $Ca_3Co_4O_9$.

DOI: 10.1103/PhysRevB.78.235107 PACS number(s): 71.28.+d, 78.70.Dm, 71.30.+h

I. INTRODUCTION

A misfit-layered Co oxide $Ca_3Co_4O_9$ contains layers of CoO_2 triangular lattice and of Ca_2CoO_3 rocksalt structure with actual composition of $[Ca_2CoO_3]_{0.62}[CoO_2]$ and shows enhanced thermopower above room temperature.[1–4] The enhanced thermopower is commonly observed in quasi-two-dimensional Co oxides with the CoO_2 triangular lattice such as Na_xCoO_2 (Refs. 5 and 6) and $Bi_2Sr_2Co_2O_9$.[7,8] A theoretical study by Koshibae *et al.*[9] explains the thermopower based on the mixed-valence state of Co^{3+} and Co^{4+} in the Co-O triangular lattice with spin and orbital degeneracy. The hopping transport of Co^{3+} and Co^{4+} species provides entropy flow that contributes to the thermopower, and the magnitude of the entropy flow depends on the spin and orbital degeneracy of Co^{3+} and Co^{4+}.

X-ray absorption and photoemission studies of the layered cobaltites including $Ca_3Co_4O_9$ showed that the hole-doped Co-O triangular lattice has spin-1/2 Co^{4+} (low-spin Co^{4+}) species in the nonmagnetic Co^{3+} (low-spin Co^{3+}) background.[10–13] In case of the Ca_2CoO_3 rocksalt layer of $Ca_3Co_4O_9$, although Masset *et al.*[1] suggested that the rocksalt layer would contain Co^{2+} species, the x-ray absorption study of $Ca_3Co_4O_9$ excluded the possibility of Co^{2+}.[11] A kink in inverse susceptibility was observed at $\sim$420 K by Masset *et al.*[1] and was assigned to a local spin-state change in the Co^{3+} species. However, Sugiyama *et al.*[14] reported that the inverse susceptibility of $Ca_3Co_4O_9$ shows a thermal hysteresis at $\sim$380 K that was assigned to a discontinuous spin-state transition from the low-spin to intermediate-spin or high-spin states of the Co^{3+} species. Single crystals were grown by a $SrCl_2$ flux method and were annealed in a O_2 flow at 450° for 12 h in the study by Sugiyama *et al.*, while, in the study by Masset *et al.*, single crystals were obtained from a mixture of K_2CO_3 and $Ca_3Co_4O_9$ powders heated up to 880° for 50 h and then slowly cooled. The fact that the transition temperature is sensitive to the difference of growing condition suggests that the spin-state transition is related to a global structural change and is not governed by a local spin-state change. In addition, the local spin-configuration change should affect the magnitude of thermopower if it exists. However, the magnitude of thermopower does not show any significant change throughout the transition at $\sim$380 K or 420 K indicating that the spin-state transition at $\sim$380 K or 420 K is different from the typical low-spin to intermediate-spin or high-spin transitions in $LaCoO_3$.[15–17]

$Ca_3Co_4O_9$ shows spin-density wave (SDW) transition at 27 K.[14,18] In the itinerant picture, the SDW transition would be due to Fermi-surface nesting. In the localized picture, the SDW transition would be governed by Co^{4+}-Co^{4+} superexchange coupling. Interestingly, substitution of Bi ions for Co ions in the rocksalt layer suppresses the SDW transition and increases the electronic specific-heat coefficient γ.[19] This indicates that the change in the rocksalt layer reduces the localization in the CoO_2 layer (in case of the localized picture) or changes the Fermi-surface geometry of the CoO_2 layer (in case of the itinerant picture).[20,21] In this context, it is highly important to study the electronic structure of $Ca_3Co_4O_9$ using photoemission spectroscopy in order to reveal to what extent the 3*d* electrons are localized in the CoO_2 layer. Also

photoemission spectroscopy would provide a useful piece of information on the valence and spin configuration of the Co ions in $Ca_3Co_4O_9$.

The angle-resolved photoemission spectroscopy (ARPES) studies of Na_xCoO_2 show the existence of relatively large hole pocket centered at Γ point indicating that the hole concentration is about 0.5 for x of 0.6–0.7.[22–24] On the other hand, the cluster-model analysis of Co $2p$ x-ray absorption spectrum (XAS) indicates that the ratio of Co^{4+} to Co^{3+} is reduced by a factor of 2 from the nominal Na content.[12] This discrepancy suggests that the systems tend to be separated into hole-rich and hole-poor domains. The hole-rich domain is a good metal and is responsible for the Fermi surface observed in ARPES and the low-temperature transport properties, while the hole-poor domain is insulating probably due to carrier localization. The ratio of Co^{4+} to Co^{3+} obtained by XAS corresponds to the average of the hole-rich and hole-poor regions. One possible scenario to explain the bad metallic behaviors of $Bi_2Sr_2Co_2O_9$ and $Ca_3Co_4O_9$ is that the volume of the hole-rich domain is small in $Bi_2Sr_2Co_2O_9$ and $Ca_3Co_4O_9$ while it is substantial in Na_xCoO_2.

In the present work, we have studied the electronic structures of $Ca_3Co_4O_9$ using x-ray photoemission spectroscopy (XPS), ultraviolet photoemission spectroscopy (UPS), and subsequent model calculations. The Co $2p$ and Co $3d$ spectra indicate that the Co $3d$ t_{2g} electrons are mostly localized supporting the phase-separation scenario. The weak spectral weight near the Fermi level probably represents the hole-rich metallic domain. The volume of which is very small compared with Na_xCoO_2. The Co $3d$ t_{2g} peak in the valence-band spectrum remains sharp even above the spin-state transition temperature of ~380 K indicating that the spin-state transition is different from the conventional low-spin to intermediate-spin (or to high-spin) transition in perovskite $LaCoO_3$.[15–17]

II. EXPERIMENT AND CALCULATION

Single crystals were grown by a flux method.[2] The XPS measurements were performed using a JPS-9200 spectrometer equipped with a monochromatized Al $K\alpha$ x-ray source ($h\nu$=1486.6 eV). The total-energy resolution was ~0.6 eV. The UPS data were taken using a SES-100 spectrometer with a He I source ($h\nu$=21.2 eV). The total-energy resolution was ~30 meV. The base pressure of the spectrometer was in the 10^{-7} Pa range. The single crystals were cleaved *in situ* in order to obtain clean surfaces. All photoemission data were collected within 12 h after the cleaving. The misfit-layered cobaltite $Ca_3Co_4O_9$ consists of the Ca(Co)-O rocksalt layer and the CoO_2 triangular lattice layer. The actual composition of $Ca_3Co_4O_9$ sample is approximately given by $[Ca_2CoO_3]_{0.62}[CoO_2]$.[2]

In the configuration-interaction approach, the ground state of the CoO_6 cluster is expressed by a linear combination of d^6, d^7L, d^8L^2, d^9L^3, and $d^{10}L^4$ configurations, where L denotes a ligand hole in the O $2p$ orbitals. The energy difference between d^6 and d^7L is given by charge-transfer energy Δ and that between d^7L and d^8L^2 by $\Delta+U$, where U is the Coulomb repulsion energy between the Co $3d$ electrons. The final states are expressed by linear combinations of cd^6, cd^7L, cd^8L^2, cd^9L^3, and $cd^{10}L^4$, where c denotes a Co $2p$ core hole. The energy difference between cd^6 and cd^7L is given by $\Delta-Q$ and that between cd^7L and cd^8L^2 by $\Delta-Q+U$, where Q is the Coulomb energy between the Co $2p$ core hole and the Co $3d$ electron. Here, the ratio U/Q is fixed at ~0.8.[25,26] The interactions between the above electronic configurations are given by the transfer integrals between the Co $3d$ and O $2p$ orbitals $(pd\sigma)$ and $(pd\pi)$. The ratio $(pd\sigma)/(pd\pi)$ is fixed to −2.16.[25,26] The Co $2p$ core-level spectrum can be calculated with the three adjustable parameters Δ, U, and $(pd\sigma)$.

In the unrestricted Hartree-Fock calculation, the CoO_2 triangular lattice is expressed by a multiband d-p Hamiltonian.[27] The Hamiltonian is given by

$$H = H_p + H_d + H_{pd},$$

$$H_p = \sum_{k,l,\sigma} \epsilon_k^p p_{k,l\sigma}^+ p_{k,l\sigma} + \sum_{k,l>l',\sigma} V_{k,ll'}^{pp} p_{k,l\sigma}^+ p_{k,l'\sigma} + \text{H.c.},$$

$$\begin{aligned} H_d = & \sum_{k,m\sigma} \epsilon_d d_{k,m\sigma}^+ d_{k,m\sigma} + \sum_{k,l>l',\sigma} V_{k,mm'}^{dd} d_{k,m\sigma}^+ d_{k,m'\sigma} + \text{H.c.} \\ & + u \sum_{i,m} d_{i,m\uparrow}^+ d_{i,m\uparrow} d_{i,m\downarrow}^+ d_{i,m\downarrow} + u' \sum_{i,m\neq m'} d_{i,m\uparrow}^+ d_{i,m\uparrow} d_{i,m'\downarrow}^+ d_{i,m'\downarrow} \\ & + (u'-j') \sum_{i,m>m',\sigma} d_{i,m\sigma}^+ d_{i,m\sigma} d_{i,m'\sigma}^+ d_{i,m'\sigma} \\ & + j' \sum_{i,m\neq m'} d_{i,m\uparrow}^+ d_{i,m'\uparrow} d_{i,m\downarrow}^+ d_{i,m'\downarrow} \\ & + j \sum_{i,m\neq m'} d_{i,m\uparrow}^+ d_{i,m'\uparrow} d_{i,m'\downarrow}^+ d_{i,m\downarrow}, \end{aligned}$$

$$H_{pd} = \sum_{k,m,l,\sigma} V_{k,lm}^{pd} d_{k,m\sigma}^+ p_{k,l\sigma} + \text{H.c.}$$

$d_{i,m\sigma}^+$ are creation operators for the $3d$ electrons at site i. $d_{k,m\sigma}^+$ and $p_{k,l\sigma}^+$ are creation operators for Bloch electrons with wave vector k which are constructed from the mth component of the Co $3d$ orbitals and from the lth component of the O $2p$ orbitals, respectively. The intra-atomic Coulomb interaction between the $3d$ electrons is expressed using Kanamori parameters u, u', j and j'.[28] Here, $u=u'+j+j'$ and $j=j'$. j is fixed to the atomic value (0.84 eV). The transfer integrals between the Co $3d$ and O $2p$ orbitals $V_{k,lm}^{pd}$ are given in terms of Slater-Koster parameters $(pd\sigma)$ and $(pd\pi)$. Here, the ratio $(pd\sigma)/(pd\pi)$ is −2.16. The transfer integrals between the O $2p$ orbitals $V_{k,ll'}^{pp}$ are expressed by $(pp\sigma)$ and $(pp\pi)$. $(pp\sigma)$ and $(pp\pi)$ are fixed at −0.60 and 0.15 eV, respectively, for the undistorted lattice. The transfer integrals between the Co $3d$ orbitals $V_{k,mm'}^{dd}$ are expressed by $(dd\sigma)$, $(dd\pi)$, and $(dd\delta)$. $(dd\sigma)$, $(dd\pi)$, and $(dd\delta)$ are fixed at −0.2, 0.1, and −0.02 eV, respectively. When the lattice is distorted, the transfer integrals are scaled using Harrison's law.[29] While the nominal charge-transfer energy is defined by $\epsilon_d^0-\epsilon_p+6U$, actual Δ is defined by $\epsilon_d^0-\epsilon_p+nU$, where ϵ_d^0 and ϵ_p are the energies of the bare $3d$ and $2p$ orbitals, n is the actual num-

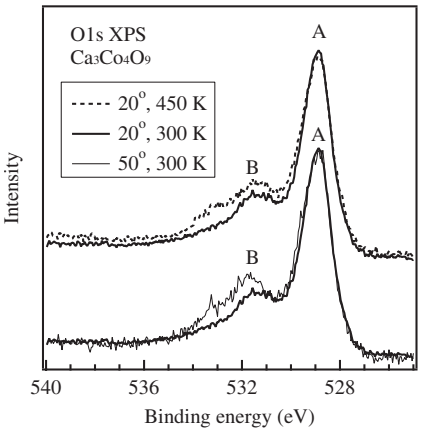

FIG. 1. O 1*s* XPS spectra of $Ca_3Co_4O_9$ taken at 300 and 450 K with $\theta=20°$ and taken at 300 K with $\theta=50°$. Here, θ is the emission angle of detected photoelectrons relative to the surface normal.

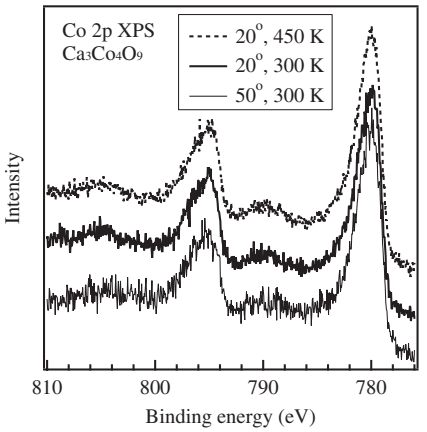

FIG. 2. Co 2*p* XPS spectra of $Ca_3Co_4O_9$ taken at 300 and 450 K with $\theta=20°$ and taken at 300 K with $\theta=50°$. Here, θ is the emission angle of detected photoelectrons relative to the surface normal.

ber of occupied 3*d* electron, and $U(=u-20/9j)$ is the multiplet-averaged *d-d* Coulomb interaction. Δ, U, and $(pd\sigma)$ for the unrestricted Hartree-Fock calculation are taken from the cluster-model analysis of the Co 2*p* spectrum.

III. RESULTS AND DISCUSSION

Figure 1 shows the O 1*s* XPS spectra of cleaved surface of $Ca_3Co_4O_9$ taken at 300 and 450 K with $\theta=20°$ and taken at 300 K with $\theta=50°$. Here, θ is the emission angle of detected photoelectrons relative to the surface normal. The cleaved surface is expected to be a mixture of the CaO rocksalt surface and the CoO_2 surface. The O 1*s* spectra consist of two structures: structure A at ~529 eV and structure B at ~531.5 eV. We have fitted the spectra to two Gaussian functions and found that the area ratio of structure A to structure B is ~0.5. It is possible to assign structure A to the CoO_2 surface and structure B to the CaO surface. The extra structure at ~533 eV is enhanced with increasing θ from 20° to 50°. This suggests that the structure at ~533 eV is due to the surface degradation. The O 1*s* spectrum taken at 450 K also has the extra structure at ~533 eV that is probably due to the degrading of the cleaved surface due to oxygen loss at elevated temperature.

Figure 2 shows the Co 2*p* XPS spectra of $Ca_3Co_4O_9$ taken at 300 and 450 K with $\theta=20°$ and taken at 300 K with $\theta=50°$. The line shape is unaffected by the difference of surface sensitivity between $\theta=20°$ and $\theta=50°$. Basically, the line shape of the Co 2*p* spectra is consistent with the low-spin configurations.[10,30,31] The main peak is somewhat broad compared to that of $Bi_2Sr_2Co_2O_9$ with the CoO_2 triangular lattice.[10] The broadening is probably due to the contribution from the Co ions in the rocksalt layer although it is difficult to decompose the spectra into the two contributions. The line shape of the Co 2*p* main peak does not change in going from 300 to 450 K, indicating that the Co^{3+} ions are dominated by the low-spin states even at 450 K.

The main peak is accompanied by the charge-transfer satellite. The intensity and the position of the charge-transfer satellite can be analyzed by the configuration-interaction calculation on the CoO_6 cluster model. Here, we assume that the Co 2*p* spectrum is dominated by the low-spin Co^{3+} contribution. This assumption is somewhat consistent with the relatively small hole concentration as pointed out by Kroll *et al.*[12] for $Na_{0.6}CoO_2$ and as estimated for $Ca_3Co_4O_9$ in the last paragraph of this section. In the configuration-interaction calculation on the CoO_6 cluster model, the ground state is expressed by a linear combination of d^6, d^7L, d^8L^2, d^9L^3, and $d^{10}L^4$ configurations and the final states are expressed by linear combinations of cd^6, cd^7L, cd^8L^2, cd^9L^3, and $cd^{10}L^4$. The Co 2*p* core-level spectrum can be calculated with the three adjustable parameters Δ, U, and $(pd\sigma)$. With $\Delta=1.0$ eV, $U=6.5$ eV, and $(pd\sigma)=-2.3$ eV, the calculated spectrum can explain the satellite structure as shown in Fig. 3. The sharpness of the satellite structure indicates that the two Co sites in the Ca_2CoO_3 rocksalt layer and the CoO_2 triangular lattice have the satellite at the same energy and that the two Co sites have similar Δ, U, and $(pd\sigma)$ values. This is consistent with the fact that the Co-O bond length in the rocksalt layer is similar to that in the CoO_2 triangular lattice.[3] The shoulders at the high-binding-energy side of Co $2p_{1/2}$ and Co $2p_{3/2}$ main peaks are due to the interaction between the clusters[32] that is not included in the present

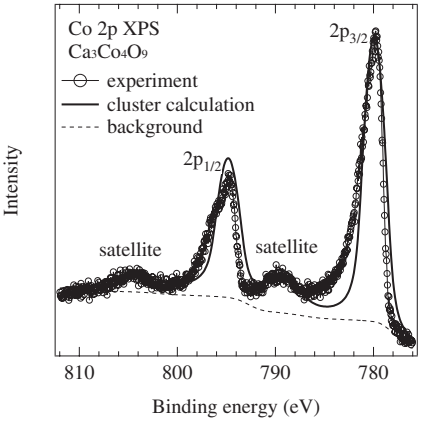

FIG. 3. Co 2*p* XPS spectrum of $Ca_3Co_4O_9$ compared with the cluster-model calculation.

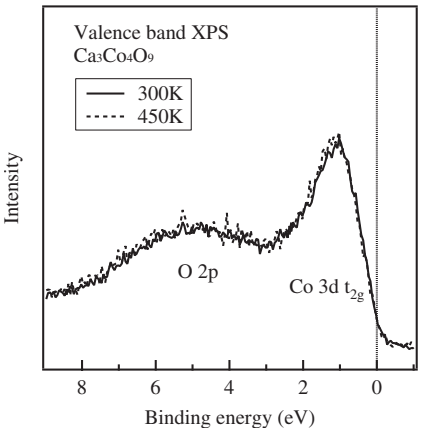

FIG. 4. Valence-band XPS spectra of $Ca_3Co_4O_9$ taken at 300 and 450 K.

single-site cluster-model calculation. For example, the shoulder structure observed in NiO can be explained by the interaction between the neighboring NiO_6 clusters.[33] However, Δ, U, and $(pd\sigma)$ are successfully obtained by the single-site cluster-model analysis.[25,26]

Figure 4 shows the valence-band XPS spectra of $Ca_3Co_4O_9$ taken at 300 and 450 K. The Co $3d$ t_{2g} peak in the valence-band spectrum also remains sharp even above the spin-state transition temperature of ~380 K. In the case of $LaCoO_3$, the Co $3d$ t_{2g} peak loses its intensity due to the transition from the low-spin to intermediate-spin or high-spin states.[31,34] This indicates that the spin-state transition at ~380 K is different from the low-spin to intermediate-spin (or high-spin) transition in $LaCoO_3$. Since the CoO_6 octahedra share their corners in perovskite, the interaction between the neighboring CoO_6 octahedra plays important roles in the spin-state transition of $LaCoO_3$. On the other hand, the CoO_6 octahedra share their edges in the CoO_2 triangular lattice of $Ca_3Co_4O_9$. Therefore, even when the intermediate- or high-spin states are thermally excited, the interaction between the neighboring intermediate-spin or high-spin states is very small and the cooperative low-spin to intermediate- or high-spin transition is not favored. Probably, the spin-state transition at 380 K in $Ca_3Co_4O_9$ does not involve any change in local spin configuration and is related to the change in the interlayer magnetic coupling.

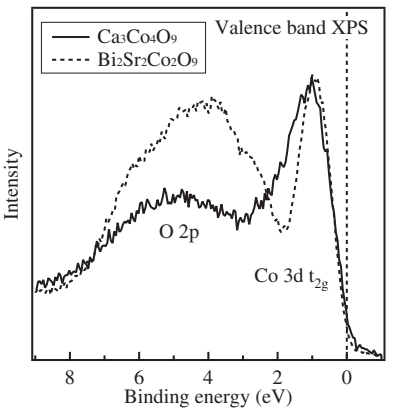

FIG. 5. Valence-band XPS spectrum of $Ca_3Co_4O_9$ compared with that of $Bi_2Sr_2Co_2O_9$.

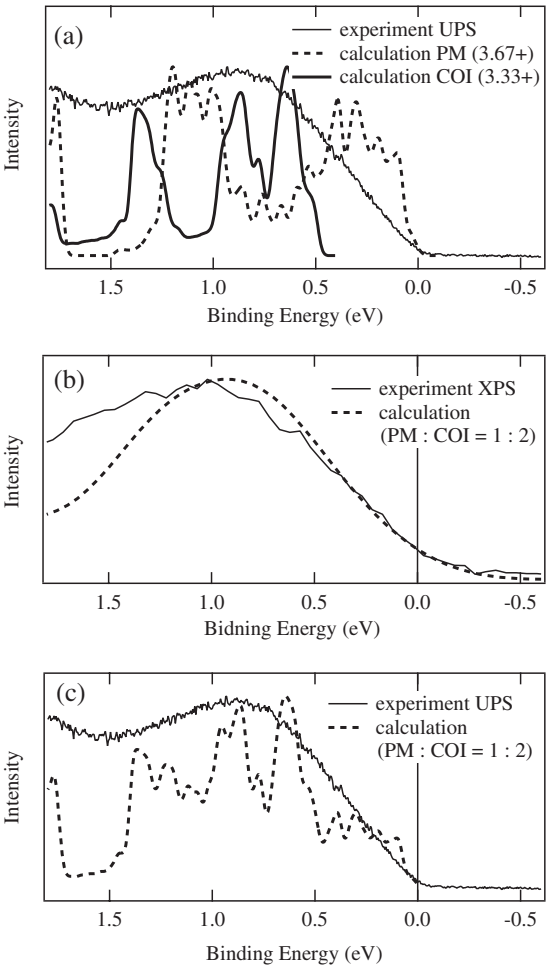

FIG. 6. (a) Valence-band UPS spectrum of $Ca_3Co_4O_9$ compared with the calculated DOS for the PM and COI states. (b) Valence-band XPS spectrum of $Ca_3Co_4O_9$ compared with the combined DOS of PM and COI states. (c) Valence-band UPS spectrum of $Ca_3Co_4O_9$ compared with the combined DOS of PM and COI states.

The Co $3d$ spectrum is dominated by the peak at ~1 eV and the spectral weight at the Fermi level is extremely weak (see Fig. 5). These spectral features indicate that the Co $3d$ t_{2g} electrons are mostly localized probably due to charge trapping or charge ordering by the structural modulation. Here, structural modulation in the Co-O bond length is mainly due to the misfit-layered structure as revealed by Miyazaki *et al.*[3] The modulation of the Co-O bond length may induce the localization of Co $3d$ t_{2g} electrons. The weak spectral weight near the Fermi level represents some metallic domains embedded in the insulating background. In order to confirm this picture, the XPS and UPS spectra near the Fermi level are compared with the density of states (DOS) calculated by the unrestricted Hartree-Fock method in Fig. 6. We have employed the multiband d-p model and performed unrestricted Hartree-Fock calculations.[27] As estimated from the cluster-model analysis of the Co $2p$ spectrum, Δ, U, and $(pd\sigma)$ for $Ca_3Co_4O_9$ are 1.0, 6.5, −2.3 eV, respectively,

whose values are more or less consistent with chemical trend obtained in various transition-metal compounds. Here, the differences of atomic subshell photoionization cross sections are considered by adding each partial DOS multiplied by their cross sections. The calculations were done not only for the paramagnetic metallic (PM) states for $Co^{3+}:Co^{4+}=1:2$ in which holes are itinerant and distributed uniformly but also for $\sqrt{3}\times\sqrt{3}$ charge-ordered insulating (COI) states for $Co^{3+}:Co^{4+}=2:1$ in which holes are localized regularly in the a_{1g} orbital to form a Wigner-type order.

First of all, the calculated result for the PM states has substantial DOS at the Fermi level that is inconsistent with the experimental result. In the next step, the combination of the PM states and the COI states is considered to reproduce the experimental result. In Fig. 6, the XPS and UPS spectra are compared with the combined DOS of PM and COI states (PM:COI=1:2) that are broadened with the experimental energy resolutions. The suppressed spectral weight at the Fermi level is successfully reproduced by the calculation. This may suggest a phase separation of PM and COI phases in $Ca_3Co_4O_9$ and $Bi_2Sr_2Co_2O_9$. Since $Ca_3Co_4O_9$ and $Bi_2Sr_2Co_2O_9$ show insulating behaviors at low temperature, it is expected that the COI phase is dominant in $Ca_3Co_4O_9$ and $Bi_2Sr_2Co_2O_9$, consistent with the above analysis. On the other hand, for Na_xCoO_2, the reported UPS spectrum has relatively high spectral weight near the Fermi level compared to that for $Ca_3Co_4O_9$.[35] Probably, the volume fraction of PM region in $Ca_3Co_4O_9$ is small compared with that in Na_xCoO_2. These results support the phase-separation scenario to understand the difference between Na_xCoO_2 and $Ca_3Co_4O_9$. The observed Fermi surface of Na_xCoO_2 is basically consistent with the prediction of local-density-approximation band-structure calculations,[20,22–24] indicating that the correlation effect is moderate in the CoO_2 layer. Therefore, it is reasonable to assume that the photoemission spectra near the Fermi level are not that different from the density of states obtained by the unrestricted Hartree-Fock approximation. The present analysis based on the unrestricted Hartree-Fock calculations is enough for the qualitative discussion on the phase separation. However, in order to reduce the difference between the theoretical and experimental results seen in Fig. 6(c) and to obtain quantitative information on the volume fraction of the metallic and insulating phases, self-energy effects beyond the Hartree-Fock approximation should be included to calculate the photoemission spectra of the metallic and insulating phases.

In the XAS study,[11] the hole concentration ratio between $Bi_2Sr_2Co_2O_9$, $Na_{0.6}CoO_2$, and $Ca_3Co_4O_9$ was found to be 0.7:1:1.5. Assuming that the hole concentration of $Na_{0.6}CoO_2$ is 0.4, those of $Bi_2Sr_2Co_2O_9$ and $Ca_3Co_4O_9$ were estimated to be 0.3 and 0.6, respectively. However, the cluster-model study by Kroll *et al.*[12] has shown that the hole concentration of $Na_{0.6}CoO_2$ is reduced by a factor of 2 from the nominal Na content. Using the corrected hole concentration of $Na_{0.6}CoO_2$ of 0.2, those of $Bi_2Sr_2Co_2O_9$ and $Ca_3Co_4O_9$ were estimated to be 0.15 and 0.3, respectively. The hole concentration of 0.3 is consistent with the actual composition $[Ca_2CoO_3]_{0.62}[CoO_2]$ (Ref. 2) that gives the average hole concentration of ~0.23.

As for the orbital population of the doped holes, the a_{1g} state is dominant in $Bi_2Sr_2Co_2O_9$ and $Ca_3Co_4O_9$ while the e_g' and a_{1g} components are heavily mixed in $Na_{0.6}CoO_2$. Unrestricted Hartree-Fock calculation on the CoO_2 triangular lattice shows that, when the doped holes are localized due to charge ordering of $Co^{3+}:Co^{4+}=2:1$, the hole state in the low-spin Co^{4+} is dominated by the a_{1g} symmetry. On the other hand, when the doped holes are itinerant and form Fermi surface as predicted by the local-density-approximation band-structure calculation,[20] the doped holes are given by mixture of e_g' and a_{1g} states. Probably, in $Bi_2Sr_2Co_2O_9$ and $Ca_3Co_4O_9$, the structural modulation induces charge localization and, consequently, the orbital state is dominated by the a_{1g} symmetry.

IV. CONCLUSION

In conclusion, we have studied the electronic structures of $Ca_3Co_4O_9$ using photoemission spectroscopy and subsequent model calculations. The cluster-model analysis of the Co $2p$ spectrum shows that the two Co sites in the Ca_2CoO_3 rock-salt layer and the CoO_2 triangular lattice layer commonly have the charge-transfer energy Δ of 1.0 eV, the d-d Coulomb interaction U of 6.5 eV, and the transfer integral $(pd\sigma)$ of −2.3 eV. The Co $2p$ and $3d$ spectra indicate that the Co $3d$ t_{2g} electrons are mostly localized. The weak spectral weight near the Fermi level is probably derived from the PM domain embedded in the COI state stabilized by the structural modulation. The volume of the PM domain is very small in $Ca_3Co_4O_9$ compared with that in Na_xCoO_2. The Co $3d$ t_{2g} peak in the valence-band spectrum remains sharp even above the spin-state transition temperature of ~380 K, indicating that the spin-state transition is different from the conventional low-spin to intermediate-spin (or to high-spin) transition in perovskite $LaCoO_3$.

ACKNOWLEDGMENT

The present work was supported by Core Research for Evolution Science and Technology (CREST) Project of the Japan Science and Technology Agency (JST).

[1] A. C. Masset, C. Michel, A. Maignan, M. Hervieu, O. Toulemonde, F. Studer, B. Raveau, and J. Hejtmanek, Phys. Rev. B **62**, 166 (2000).

[2] Y. Miyazaki, K. Kudo, M. Akoshima, Y. Ono, Y. Koike, and T. Kajitani, Jpn. J. Appl. Phys., Part 2 **39**, L531 (2000).

[3] Y. Miyazaki, M. Onoda, T. Oku, M. Kikuchi, Y. Ishii, Y. Ono, Y. Morii, and T. Kajitani, J. Phys. Soc. Jpn. **71**, 491 (2002).

[4] S. Lambert, H. Leligny, and D. Grebille, J. Solid State Chem. **160**, 322 (2001).

[5] I. Terasaki, Y. Sasago, and K. Uchinokura, Phys. Rev. B **56**,

R12685 (1997).
[6] K. Fujita, T. Mochida, and K. Nakamura, Jpn. J. Appl. Phys., Part 1 **40**, 4644 (2001).
[7] T. Yamamoto, I. Tsukada, K. Uchinokura, M. Takagi, T. Tsubone, M. Ichihara, and K. Kobayashi, Jpn. J. Appl. Phys., Part 2 **39**, L747 (2000).
[8] H. Leligny, D. Grebille, O. Pérez, A. Masset, M. Hervieu, C. Michel, B. Raveau, and C.R. Acad. Sci., Ser. IIc: Chim **2**, 409 (1999).
[9] W. Koshibae and S. Maekawa, Phys. Rev. Lett. **87**, 236603 (2001); W. Koshibae, K. Tsutsui, and S. Maekawa, Phys. Rev. B **62**, 6869 (2000).
[10] T. Mizokawa, L. H. Tjeng, P. G. Steeneken, N. B. Brookes, I. Tsukada, T. Yamamoto, and K. Uchinokura, Phys. Rev. B **64**, 115104 (2001).
[11] T. Mizokawa, L. H. Tjeng, H.-J. Lin, C. T. Chen, R. Kitawaki, I. Terasaki, S. Lambert, and C. Michel, Phys. Rev. B **71**, 193107 (2005).
[12] T. Kroll, A. A. Aligia, and G. A. Sawatzky, Phys. Rev. B **74**, 115124 (2006).
[13] T. Kroll, M. Knupfer, J. Geck, C. Hess, T. Schwieger, G. Krabbes, C. Sekar, D. R. Batchelor, H. Berger, and B. Buchner, Phys. Rev. B **74**, 115123 (2006).
[14] J. Sugiyama, C. Xia, and T. Tani, Phys. Rev. B **67**, 104410 (2003).
[15] M. Abbate, J. C. Fuggle, A. Fujimori, L. H. Tjeng, C. T. Chen, R. Potze, G. A. Sawatzky, H. Eisaki, and S. Uchida, Phys. Rev. B **47**, 16124 (1993).
[16] M. A. Korotin, S. Yu. Ezhov, I. V. Solovyev, V. I. Anisimov, D. I. Khomskii, and G. A. Sawatzky, Phys. Rev. B **54**, 5309 (1996).
[17] M. W. Haverkort, Z. Hu, J. C. Cezar, T. Burnus, H. Hartmann, M. Reuther, C. Zobel, T. Lorenz, A. Tanaka, N. B. Brookes, H. H. Hsieh, H.-J. Lin, C. T. Chen, and L. H. Tjeng, Phys. Rev. Lett. **97**, 176405 (2006).
[18] J. Sugiyama, J. H. Brewer, E. J. Ansaldo, H. Itahara, K. Dohmae, Y. Seno, C. Xia, and T. Tani, Phys. Rev. B **68**, 134423 (2003).
[19] P. Limelette, V. Hardy, P. Auban-Senzier, D. Jerome, D. Flahaut, S. Hebert, R. Fresard, Ch. Simon, J. Noudem, and A. Maignan, Phys. Rev. B **71**, 233108 (2005).
[20] D. J. Singh, Phys. Rev. B **61**, 13397 (2000).
[21] R. Asahi, J. Sugiyama, and T. Tani, Phys. Rev. B **66**, 155103 (2002).
[22] M. Z. Hasan, Y. D. Chuang, D. Qian, Y. W. Li, Y. Kong, A. P. Kuprin, A. V. Fedorov, R. Kimmerling, E. Rotenberg, K. Rossnagel, Z. Hussain, H. Koh, N. S. Rogado, M. L. Foo, and R. J. Cava, Phys. Rev. Lett. **92**, 246402 (2004).
[23] H. B. Yang, S. C. Wang, A. K. P. Sekharan, H. Matsui, S. Souma, T. Sato, T. Takahashi, T. Takeuchi, J. C. Campuzano, R. Jin, B. C. Sales, D. Mandrus, Z. Wang, and H. Ding, Phys. Rev. Lett. **92**, 246403 (2004).
[24] H. B. Yang, Z. H. Pan, A. K. P. Sekharan, T. Sato, S. Souma, T. Takahashi, R. Jin, B. C. Sales, D. Mandrus, A. V. Fedorov, Z. Wang, and H. Ding, Phys. Rev. Lett. **95**, 146401 (2005).
[25] K. Okada and A. Kotani, J. Phys. Soc. Jpn. **60**, 772 (1991).
[26] A. E. Bocquet, T. Mizokawa, T. Saitoh, H. Namatame, and A. Fujimori, Phys. Rev. B **46**, 3771 (1992).
[27] T. Mizokawa and A. Fujimori, Phys. Rev. B **54**, 5368 (1996).
[28] J. Kanamori, Prog. Theor. Phys. **30**, 275 (1963).
[29] W. A. Harrison, *Electronic Structure and the Properties of Solids* (Dover, New York, 1989).
[30] J. van Elp, J. L. Wieland, H. Eskes, P. Kuiper, G. A. Sawatzky, F. M. F. de Groot, and T. S. Turner, Phys. Rev. B **44**, 6090 (1991).
[31] T. Saitoh, T. Mizokawa, A. Fujimori, M. Abbate, Y. Takeda, and M. Takano, Phys. Rev. B **56**, 1290 (1997).
[32] M. A. van Veenendaal and G. A. Sawatzky, Phys. Rev. Lett. **70**, 2459 (1993).
[33] S. Altieri, L. H. Tjeng, A. Tanaka, and G. A. Sawatzky, Phys. Rev. B **61**, 13403 (2000).
[34] Z. Hu, H. Wu, M. W. Haverkort, H. H. Hsieh, H.-J. Lin, T. Lorenz, J. Baier, A. Reichl, I. Bonn, C. Felser, A. Tanaka, C. T. Chen, and L. H. Tjeng, Phys. Rev. Lett. **92**, 207402 (2004).
[35] T. Takeuchi, T. Kondo, T. Takami, H. Takahashi, H. Ikuta, U. Mizutani, K. Soda, R. Funahashi, M. Shikano, M. Mikami, S. Tsuda, T. Yokoya, S. Shin, and T. Muro, Phys. Rev. B **69**, 125410 (2004).